

The determination of the three-dimensional structure of barley serine proteinase inhibitor 2 by nuclear magnetic resonance, distance geometry and restrained molecular dynamics

G.Marius Clore², Angela M.Gronenborn, Mogens Kjaer¹, and Flemming M.Poulsen^{1,2}

¹Max-Planck Institut für Biochemie, D-8033 Martinsried bei München, FRG and ²Department of Chemistry, The Carlsberg Laboratory, Gamle Carlsbergvej 10, DK-2500 Valby Copenhagen, Denmark

²Authors to whom reprint requests should be sent

The solution structure of the 64 residue structured domain (residues 20–83) of barley serine proteinase inhibitor 2 (BSPI-2) is determined on the basis of 403 interproton distance, 34 ϕ backbone torsion angle and 26 hydrogen bonding restraints derived from n.m.r. measurements. A total of 11 converged structures were computed using a metric matrix distance geometry algorithm and refined by restrained molecular dynamics. The average rms difference between the final 11 structures and the mean structure obtained by averaging their coordinates is $1.4 \pm 0.2 \text{ \AA}$ for the backbone atoms and $2.1 \pm 0.1 \text{ \AA}$ for all atoms. The overall structure, which is almost identical to that found by X-ray crystallography, is disc shaped and consists of a central four component mixed parallel and antiparallel β -sheet flanked by a 13 residue α -helix on one side and the reactive site loop on the other.

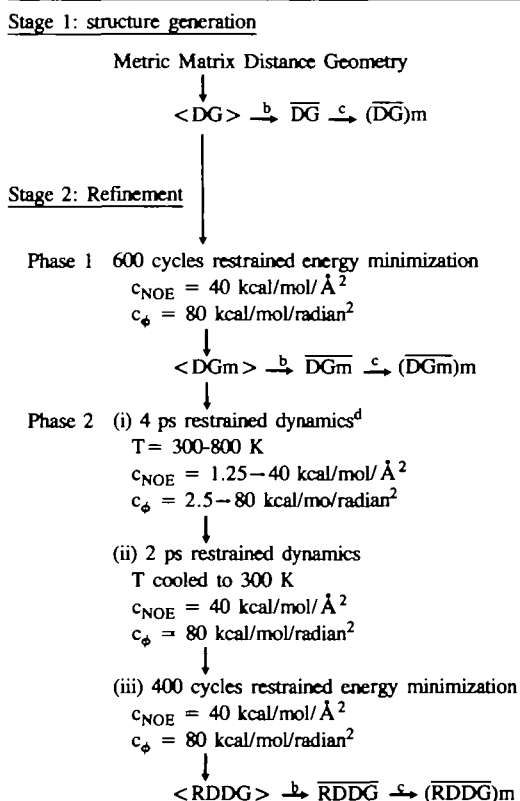
Key words: Barley serine protease inhibitor/solution structure/nuclear Overhauser effect/interproton distances/distance geometry/restrained molecular dynamics

Introduction

Barley serine proteinase inhibitor 2 (BSPI-2, also known as chymotrypsin inhibitor 2, CI-2) is a small 83 residue protein with no disulphide bridges (Jonassen, 1980; Svendsen *et al.*, 1980) which is a member of the potato inhibitor 1 family of serine proteinase inhibitors (Laskowski and Kato, 1980). Recently, the crystal structure of the complex of BSPI-2 and subtilisin Novo (MacPhalen *et al.*, 1985) as well as that of the native inhibitor (McPhalen and James, 1987) have been solved. Independently of the crystallographic studies, an n.m.r. study was undertaken with the eventual aim of determining the three-dimensional structure of BSPI-2 in solution. This has led to the sequential assignment of the ¹H-n.m.r. spectrum of BSPI-2 (Kjaer *et al.*, 1987) and the delineation of regular structural elements on the basis of a qualitative interpretation of nuclear Overhauser enhancement (NOE) data (Kjaer and Poulsen, 1987). In this paper, the n.m.r. study is extended to the determination of the three-dimensional structure of the 64 residue proteolytic fragment of BSPI-2 (residues 20–83) on the basis of approximate interproton distance, ϕ backbone torsion angle and hydrogen bonding restraints, using a combination of metric matrix distance geometry (Crippen and Havel, 1975; Havel *et al.*, 1983; Havel and Wüthrich, 1984, 1985; Sippl and Scheraga, 1986) and restrained molecular dynamics (Kaptein *et al.*, 1985; Clore *et al.*, 1985, 1986a,b; Brünger *et al.*, 1986) calculations. The choice of the 64 residue proteolytic fragment rather than the intact protein was based on the fact that the first 19 residues are disordered both

in solution (Kjaer *et al.*, 1987; Kjaer and Poulsen, 1987) and in the crystal structures (McPhalen *et al.*, 1985; MacPhalen and James, 1987). In the following paper (Clore *et al.*, 1987a) a detailed comparison of the solution and crystal structures is presented.

Table I. Protocol used for the determination of the three-dimensional structure of BSPI-2^a



^aThe notation of the structures is as follows: $\langle \text{DG} \rangle$ comprise the 11 converged distance geometry structures, $\langle \text{DGm} \rangle$ the structures derived from the $\langle \text{DG} \rangle$ structures by restrained energy minimization, and $\langle \text{RDDG} \rangle$ the structures derived from the $\langle \text{DGm} \rangle$ structures by restrained molecular dynamics.

^bThe structure $\overline{\text{DG}}$, $\overline{\text{DGm}}$ and $\overline{\text{RDDG}}$ are obtained by averaging the coordinates of the $\langle \text{DG} \rangle$, $\langle \text{DGm} \rangle$ and $\langle \text{RDDG} \rangle$ structures, respectively, best fitted to residues 22–83.

^cThe structures $(\overline{\text{DG}})_m$, $(\overline{\text{DGm}})_m$ and $(\overline{\text{RDDG}})_m$ were derived from the average structures $\overline{\text{DG}}$, $\overline{\text{DGm}}$ and $\overline{\text{RDDG}}$, respectively, by 600 cycles of restrained energy minimization in which the van der Waals radii were increased gradually from a quarter of their usual values to their full values in order to overcome the very bad non-bonded contacts present in the average structures (Clore *et al.*, 1986a).

^dThe temperature of the system was adjusted to lie between 300 K and 800 K by scaling the velocities of the atoms upwards by a factor of 1.25 if the temperature fell below 300 K and downwards by a factor of 0.75 if the temperature rose above 800 K. The velocity scaling was carried out every 0.25 ps. The NOE (c_{NOE}) and ϕ backbone torsion angle (c_{ϕ}) restraints force constants were increased from 1.25 kcal/mol/ \AA^2 up to a maximum value of 40 kcal/mol/ \AA^2 and from 2.5 kcal/mol/radian² up to a maximum value of 80 kcal/mol/radian², respectively, by doubling their value every 0.25 ps.

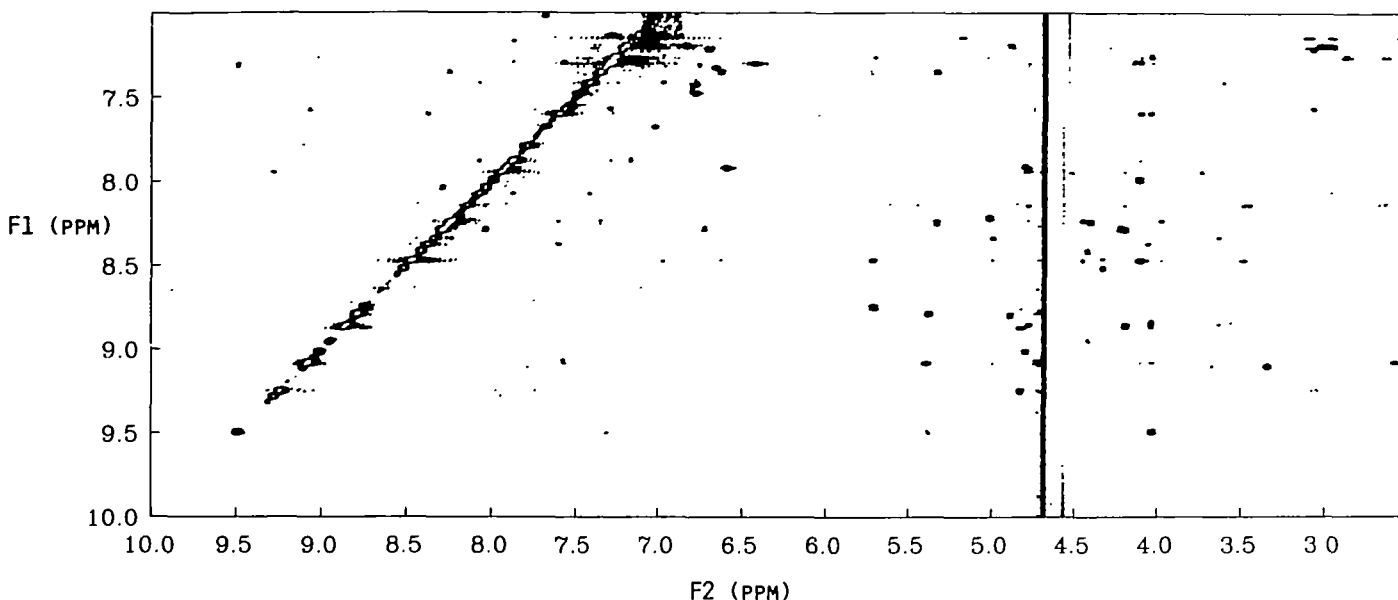


Fig. 1. NH/aromatic (F1 axis)-NH/aromatic/aliphatic (F2 axis) region of the 200 ms NOESY spectrum of BSPI-2 in 90% H₂O/10% D₂O at 42°C.

Table II. Atomic rms differences^a

	Atomic rms differences (Å) for residues 22–83 ^b	
	Backbone atoms	All atoms
(A) Rms distributions		
<DG> vs <DG>	1.58 ± 0.14	2.65 ± 0.18
<DGm> vs <DGm>	1.55 ± 0.14	2.60 ± 0.19
<RDDG> vs <RDDG>	2.10 ± 0.27	3.10 ± 0.27
<DG> vs $\overline{\text{DG}}^c$	1.09 ± 0.09	1.82 ± 0.13
<DGm> vs $\overline{\text{DGm}}^c$	1.06 ± 0.10	1.79 ± 0.13
<RDDG> vs $\overline{\text{RDDG}}^c$	1.43 ± 0.18	2.13 ± 0.14
<DG> vs $(\overline{\text{DG}})_m$	1.29 ± 0.12	2.07 ± 0.14
<DGm> vs $(\overline{\text{DGm}})_m$	1.23 ± 0.12	2.01 ± 0.15
<RDDG> vs $(\overline{\text{RDDG}})_m$	1.57 ± 0.19	2.32 ± 0.19
(B) Rms shifts		
<DG> vs <DGm>	0.43 ± 0.04	0.44 ± 0.03
<DGm> vs <RDDG>	1.85 ± 0.27	2.40 ± 0.30
<DG> vs <RDDG>	1.96 ± 0.24	2.51 ± 0.29
$\overline{\text{DG}}$ vs $\overline{\text{DGm}}$	0.28	0.28
$\overline{\text{DGm}}$ vs $\overline{\text{RDDG}}$	1.24	1.49
$\overline{\text{DG}}$ vs $\overline{\text{RDDG}}$	1.96	2.51
$\overline{\text{DG}}$ vs $(\overline{\text{DG}})_m$	0.71	0.97
$\overline{\text{DGm}}$ vs $(\overline{\text{DGm}})_m$	0.62	0.89
$\overline{\text{RDDG}}$ vs $(\overline{\text{RDDG}})_m$	0.63	0.98
$(\overline{\text{DG}})_m$ vs $(\overline{\text{DGm}})_m$	0.28	0.41
$(\overline{\text{DGm}})_m$ vs $(\overline{\text{RDDG}})_m$	1.31	1.79
$(\overline{\text{DG}})_m$ vs $(\overline{\text{RDDG}})_m$	1.37	1.83

^aThe notation of the structures is the same as that in Table I.

^bThe reason that residues 20 and 21 are excluded from the atomic rms differences is that their conformation could not be determined as no NOEs involving these two residues were observed.

^cThe estimated standard atomic rms errors s_{mean} of the mean structures is given by $[\sum(\text{rmsd}_i)^2/n(n-1)]^{1/2}$ where rmsd_i is the atomic rms difference between the *i*th structure and the mean structure and *n* is the number of structures.

Materials and methods

The 64 residue proteolytic fragment of BSPI-2 was prepared as described previously (Jonassen, 1980; Svendsen *et al.*, 1980). Samples for n.m.r. contained 8 mM BSPI-2 in either 90% H₂O/10% D₂O or 99.996% D₂O pH 4.2. Two-dimensional nuclear Overhauser enhancement spectroscopy (NOESY) spectra (Jeener *et al.*, 1979; Macura *et al.*, 1981) were recorded in pure phase adsorption mode (States *et al.*, 1982) using the experimental conditions reported previously (Kjaer *et al.*, 1987). Measurements were carried out at 22, 37 and 42°C.

Metric matrix distance geometry calculations were carried out with the program DISGEO (Havel and Wüthrich, 1984, 1985; Havel, 1986). All energy minimization and restrained molecular dynamics calculations were carried out as described previously (Clore *et al.*, 1986a,b) on a CONVEX-C1XP using the program XPLOR (A.T.Brünger, unpublished data) which is a vectorised version of the program CHARMM (Brooks *et al.*, 1983) especially adapted for restrained molecular dynamics. Displaying of the structures was carried out using a modified version of the function network of FRODO (Jones, 1978) interfaced with XPLOR on an Evans and Sutherland PS330 colour graphic system. The smooth backbone (N, C^α, C) atom representations were obtained as described previously (Feldman *et al.*, 1986).

Results and Discussions

Restraints

The basis of the structure determination consisted of a set of 403 approximate interproton distance restraints comprising 140 short ($|i-j| \leq 5$) and 70 long ($|i-j| \geq 5$) range interresidue distances and 193 intraresidue distances. These were derived from pure phase absorption NOESY spectra recorded with mixing times of 100, 150 and 200 ms. An example of the quality of the NOESY spectra is shown in Figure 1. All the NOEs were classified into three distance ranges, 1.8–2.7 Å, 1.8–3.3 Å and 1.8–5.0 Å, corresponding to strong, medium and weak NOEs (Williamson *et al.*, 1985). In the case of NOEs involving methyl groups an additional 0.5 Å per methyl group was added to the upper distance limit to account for the higher apparent intensity of methyl resonances (Clore *et al.*, 1987b).

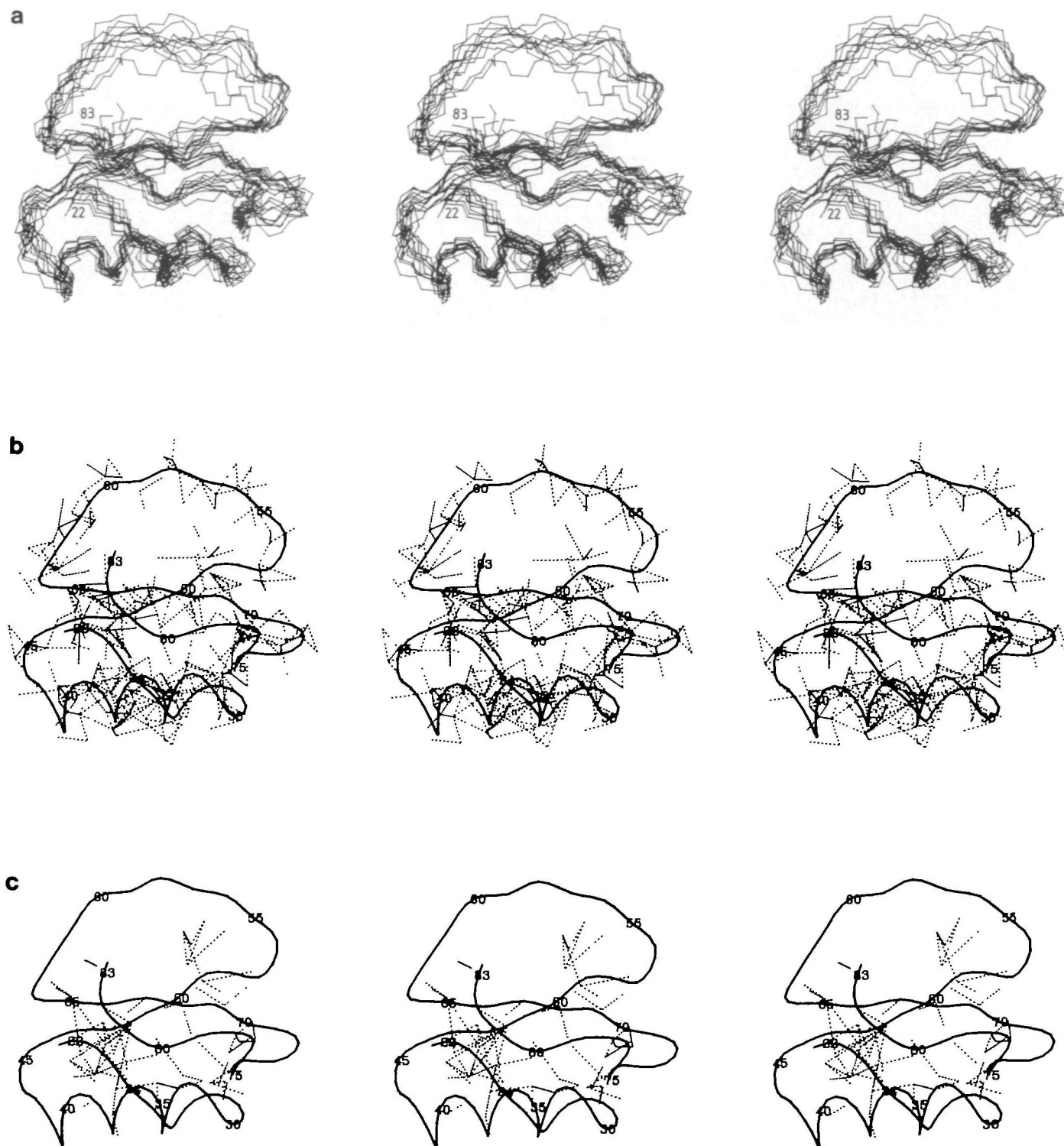


Fig. 2. (a) Best-fit superposition of the backbone (C, C α , N) atoms of the 11 converged RDDG structures (residues 22–83). (b) and (c) The short and long range interproton distances restraints shown as dashed lines, respectively, superimposed on a framework comprising a smoothed backbone (C, C α , N) atom representation of the restrained energy minimized average structure (RDDG)m.

The NOE interproton distance restraints were supplemented by two additional sets of restraints. The first set consisted of 34 ϕ backbone torsion angle restraints derived from $^3J_{\text{HN}\alpha}$ coupling constants (Pardi *et al.*, 1984) measured from a double quantum filtered two-dimensional homonuclear correlated (DQF-COSY) spectrum in H₂O. Of these, 20 were restrained to the range -80° to -180° on the basis of apparent values of $^3J_{\text{HN}\alpha}$

> 9 Hz, while 14 were restrained to the range -10° to -90° on the basis of apparent values of $^3J_{\text{HN}\alpha} < 6$ Hz (Kjaer and Poulsen, 1987). The second set consisted of 26 distance restraints derived on the basis of 13 backbone hydrogen bonds identified in the mixed parallel/antiparallel β -sheet on the basis of a qualitative interpretation of the NOE data and amide exchange data (Kjaer and Poulsen, 1987). Each hydrogen bond was

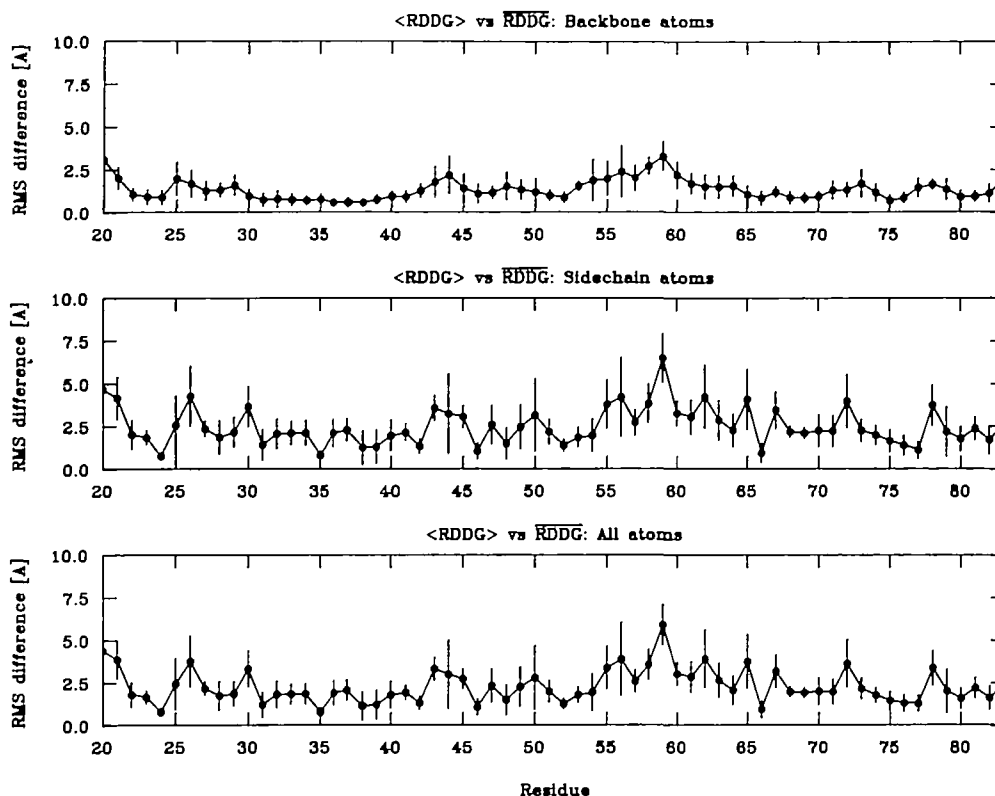


Fig. 3. Atomic rms distribution of the backbone (C,C α ,N,O) atoms, side-chain atoms and all atoms of the 11 RDDG structures about the mean structure $\overline{\text{RDDG}}$ best fitted to residues 22–83. The filled-in circles (\bullet) represent the average rms difference at each residue between the <RDDG> structures and the mean RDDG structure, and the bars represent the standard deviations in these values.

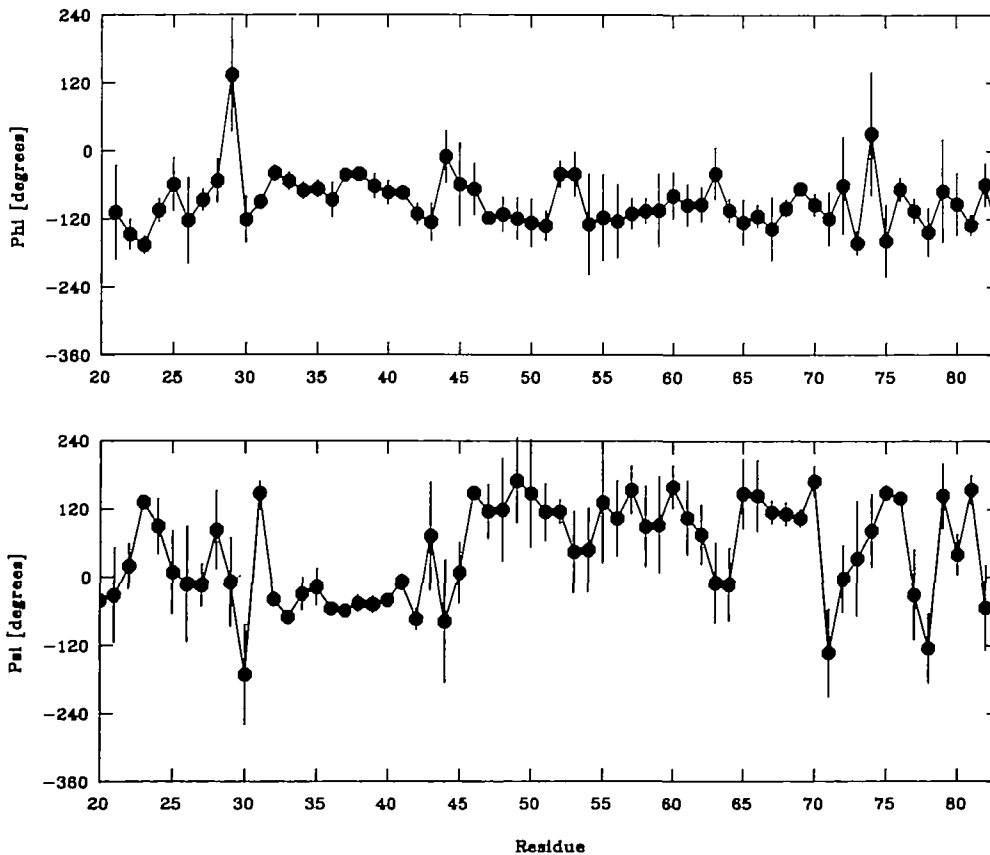


Fig. 4. Angular rms distribution of the ϕ and ψ backbone torsion angles of the <RDDG> structures. The filled in circles (\bullet) are the values of the ϕ and ψ angles of the restrained energy minimized average structure ($\overline{\text{RDDG}}$)_m and the bars represent the average angular rms deviations between the pairs of RDDG structures.

Table III. Interproton distance deviations and radii of gyration^a

Structure	Rms difference between calculated and target interproton distance restraints (Å)			Radii of gyration (Å)	
	All (403)	Interresidue		Intraresidue (193)	
		short range ($ i-j \leq 5$) (140)	long range ($ i-j > 5$) (70)		
<DG>	0.56 ± 0.03	0.55 ± 0.05	0.92 ± 0.10	0.36 ± 0.03	11.57 ± 0.13
<DGm>	0.18 ± 0.02	0.19 ± 0.02	0.23 ± 0.41	0.15 ± 0.01	11.49 ± 0.13
<RDDG>	0.11 ± 0.01	0.12 ± 0.01	0.11 ± 0.02	0.09 ± 0.01	10.96 ± 0.14
$\overline{\text{DG}}$	0.43	0.41	0.75	0.26	11.41
$\overline{\text{DGm}}$	0.24	0.25	0.35	0.17	11.34
$\overline{\text{RDDG}}$	0.19	0.20	0.22	0.18	10.75
$(\overline{\text{DG}})_m$	0.12	0.15	0.09	0.11	11.52
$(\overline{\text{DGm}})_m$	0.12	0.14	0.09	0.12	11.49
$(\overline{\text{RDDG}})_m$	0.09	0.11	0.07	0.09	10.98

^aThe notation of the structures is the same as that in Table I. The rms difference (rmsd) between the calculated (r_{ij}) and target restraints is calculated with respect to the upper (r_{ij}^u) and lower (r_{ij}^l) limits such that

$$\text{rmsd} = \begin{cases} [(r_{ij} - r_{ij}^u)^2/n]^{1/2} & , \text{ if } r_{ij} > r_{ij}^u \\ 0 & , \text{ if } r_{ij}^l \leq r_{ij} \leq r_{ij}^u \\ [(r_{ij} - r_{ij}^l)^2/n]^{1/2} & , \text{ if } r_{ij} < r_{ij}^l \end{cases}$$

Table IV. Energies of the structures^a

Structure	Energy (kcal/mol)										
	Total	Potential	Bond (1069)	Angle (1961)	Dihedral (528)	Improper (265)	van der Waals	Electrostatic	H-bond	NOE restraints ^b (403)	ϕ torsion restraints ^b (34)
<DG>	7104 ± 755	1925 ± 732	132 ± 31	566 ± 77	510 ± 27	0.4 ± 0.5	776 ± 669	-162 ± 41	-18 ± 6	5104 ± 497	194 ± 69
<DGm>	1275 ± 199	738 ± 143	137 ± 23	659 ± 58	446 ± 18	0.3 ± 0.1	-17 ± 49	-478 ± 37	-33 ± 4	531 ± 79	23 ± 10
<RDDG>	-167 ± 116	-360 ± 91	81 ± 11	478 ± 48	326 ± 14	0.1 ± 0.02	-145 ± 26	-1040 ± 50	-61 ± 6	184 ± 26	9 ± 5
$\overline{\text{DG}}$	> 10 ⁶	> 10 ⁶	29631	7580	1079	0.4	> 10 ⁶	-592	-23	2999	199
$\overline{\text{DGm}}$	> 10 ⁶	> 10 ⁶	28259	6641	1161	1.4	> 10 ⁶	-644	-27	918	255
$\overline{\text{RDDG}}$	> 10 ⁶	> 10 ⁶	30509	6752	1063	10.6	> 10 ⁶	-18522	-38	601	5
$(\overline{\text{DG}})_m$	866	633	112	619	463	0.2	9	-534	-36	227	6
$(\overline{\text{DGm}})_m$	833	575	105	639	458	0.1	5	-593	-39	244	14
$(\overline{\text{RDDG}})_m$	228	81	82	502	407	0.2	-85	-767	-59	142	5

^aThe notation of the structures is the same as that in Table I. The total energy is the sum of the potential and restraints (NOE and ϕ) energies, and the potential energy is made up of all the other bonded and non-bonded energy terms. The number of terms for the bond, angle dihedral and improper dihedral (planarity) potentials and for the effective NOE interproton distance and ϕ backbone torsion angle restraints potential is given in parentheses.

^bThe NOE and ϕ torsion angle restraints force constants (cf Eq. 1 of Clore *et al.*, 1986b) have values of 40 kcal/mol/Å² and 80 kcal/mol/radian², respectively.

represented by two distance restraints, namely $\text{N} \cdots \text{O} \leq 3.3 \text{ \AA}$ and $\text{NH} \cdots \text{O} \leq 2.3 \text{ \AA}$.

Tertiary structure computation

The tertiary structure computation followed the same two-stage approach that we have previously used on other proteins (Clore *et al.*, 1986b, 1987b,c,d,e), namely a structure generation stage using the metric matrix distance geometry program DISGEO (Havel, 1986), followed by a refinement stage using a combination of restrained energy minimization and restrained molecular dynamics in which the experimental restraints are incorporated as effective potentials into the total energy of the system (Levitt, 1983; Kaptein *et al.*, 1985; Clore *et al.*, 1985, 1986a; Brünger *et al.*, 1986). The protocol employed, together with the notation of the structures, is summarized in Table I. Three features are noteworthy: (i) in the distance geometry calculations all the ex-

perimental restraints are included explicitly in the calculations, whereas in the refinement stage the hydrogen bonding distance restraints are not included explicitly in the restraints effective potential as they are represented by the hydrogen bonding potential of the empirical energy function; (ii) the upper limits of distances involving methyl and methylene protons are corrected for the pseudo-atom representation (Wüthrich *et al.*, 1983) in the distance geometry calculations, but are uncorrected in the refinement stage as they are represented by single ($\langle r^{-6} \rangle$)^{-1/6} average distances; (iii) the form of the effective potentials used to describe the experimental restraints is a square-well (Clore *et al.*, 1986b).

The converged structures

A total of 11 converged DG structures were generated and subjected to refinement. The course of the refinement is summariz-

Table V. ϕ, ψ angular rms differences and violations for the converged DG, DGm and RDDG structures

Structure	rmsd $_{\phi}$ (°)	viol $_{\phi}$ (residues)	rmsd $_{\psi}$ (°)	viol $_{\psi}$ (residues)
<DG> vs <DG>	41 ± 21	9 (29,45,46, 56,59,72, 74,78,89)	47 ± 26	7 (43,44,59, 63,71,83, 82)
<DGm> vs <DGm>	35 ± 19	6 (26,29,56, 72,74,79)	44 ± 24	9 (43,44,54, 55,59,71, 73,77,82)
<RDDG> vs <RDDG>	34 ± 21	4 (29,74,79, 83)	44 ± 26	7 (26,43,44, 48,50,55, 73)

The angular violations are defined as the number of angles for which the average rms difference between the structures is greater than 90°; these angles are not included in the calculation of the average angular rms difference. The residues where the angular violations occur are shown in brackets. The notation for the structures is the same as that in Table I.

ed in Tables II–V which give the atomic root mean square (rms) distributions and shifts, the interproton distance deviations and radii of gyration, the energies of the structures, and the ϕ, ψ angular rms differences, respectively. The best fit superposition of the backbone (N, C $^{\alpha}$, C) atoms of the final 11 RDDG structures is shown in Figure 2 together with the superposition of the short ($|i-j| \leq 5$) and long ($|i-j| > 5$) range interproton distances superimposed on a smoothed backbone atom representation of the restrained energy minimized average structure (RDDG)m.

As in the case of previous structure determinations (Clore *et al.* 1986b, 1987b,c,d,e) the effect of refinement is to improve the structures not only with respect to their agreement with the experimental interproton distances (Table II and IV) but also with respect to their stereochemistry and non-bonded contacts (Table IV). The initial restrained energy minimization phase of the refinement simply takes the <DG> structures into the next local minimum and is thus associated with only small (~0.4 Å) backbone atomic rms shifts (Table III). The restrained molecular dynamics phase of the refinement, on the other hand, samples the lowest energy subminima in the global minimum energy region and is associated with much larger (~1.9 Å) backbone atomic rms shifts (Table III). Associated with this is an increase in the atomic rms distribution of the <RDDG> structures about the mean structure RDDG relative to that of the <DG> or <DGm> structures about their respective means (Table III). This increase in the atomic rms distribution, however, is not manifested in the angular distribution of the backbone ϕ, ψ angles, which is in fact slightly reduced, particularly in terms of the numbers of angles deviating by more than 90° between structures (Table V). It is also worth pointing out, that although the average structures themselves are very poor in energetic terms, they are located in the neighbourhood of local subminima whose energies are comparable to those of the individual structures from which the mean structures are derived. Thus, the hierarchy of energies of the restrained energy minimized average structures follows that of the individual structures, with (RDDG)m having the lowest energy and (DG)m the highest (Table IV).

Structural features

The structural features of BSPI-2 are best appreciated from the stereoviews shown in Figure 2. It is a disc shaped protein com-

posed of a central 4-component mixed parallel and antiparallel β -sheet, flanked by a helix (residues 32–43) on one side, and the reactive site loop (residues 54–62) on the other. The β -sheet is composed of six strands (residues 22–24, 30–32, 47–53, 64–70, 74–77 and 80–82) and a number of turns. Three overlapping turns (24–27, type III; 25–28, type I; and 27–30, type II) connect strands 1 and 2. Type I turns connect the helix and strand 3 (residues 43–46), the C-terminal end of the reactive site loop and strand 4 (residues 62–65), and strands 4 and 5 (residues 71–74). Strands 5 and 6 are connected by a 'half-turn' (residues 78–79). Strands 1 and 6, 2 and 5, and 4 and 5 are antiparallel, and strand 3 is parallel to strand 4. The four separate components of the mixed parallel/antiparallel β -sheet are thus formed by (i) strands 1 and 2, (ii) strand 3, (iii) strand 4, and (iv) strands 5 and 6. These results confirm the picture of the secondary structure deduced from a qualitative interpretation of the NOE data (Kjaer and Poulsen, 1987). In addition, most of these structural features are also found in the X-ray structures of BSPI-2 (McPhalen *et al.*, 1985; McPhalen and James, 1987), a comparison with which is presented in the following paper (Clore *et al.*, 1987a).

Examination of the backbone atomic rms distribution of the <RDDG> structures about the mean structure RDDG (Figure 3) shows that the regular secondary structure elements (β -sheet and α -helix) are well determined with an average backbone atomic rms distribution of ≤ 1 Å. This is also extended to the ϕ and ψ backbone torsion angles (Figure 4). The atomic rms distribution of the loop residues is slightly larger but its orientation with respect to the β -sheet is well defined, in contrast to the case of hirudin (Clore *et al.*, 1987c). The reason for this lies in the fact that the location of the loop in BSPI-2 is fixed by NOEs bridging the hinges connecting the loop to the main body of the protein: in particular between Phe 69 of strand 4 on the one hand and Thr 55 and Val 57 of the loop on the other, and between Gly 83 of strand 6 and Tyr 61 of the loop. It will also be noted that the atomic rms distribution for residues 20 and 21 is very large. This is simply due to the fact that no NOEs involving these residues were observed so that their positions are not constrained by experimental data.

Considering the side chain atoms, we note that their atomic rms distribution is ~50% larger than that of the backbone atoms (Figure 3). This is particularly marked for surface side chains (e.g. in the reactive site loop), as the definition of their positions, in contrast to those of internal side chains, is not aided by the restrictions imposed by packing requirements within the protein interior.

Acknowledgements

This work was supported by the Max-Planck Gesellschaft and Grant No. 321/4003/0318909A from the Bundesministerium für Forschung und Technologie (G.M.C. and A.M.G.). The Bruker AM500 n.m.r. spectrometer was provided by the Danish Natural Science Council and the Carlsberg Foundation (F.M.P. and M.K.).

References

- Brooks, B.R., Brucoleri, R.E., Olafson, B.D., States, D.J., Swaminathan, S. and Karplus, M. (1983) *J. Comput. Chem.*, **4**, 187–217.
- Brünger, A.T., Clore, G.M., Gronenborn, A.M. and Karplus, M. (1986) *Proc. Natl. Acad. Sci. USA*, **83**, 3801–3805.
- Clore, G.M., Gronenborn, A.M., Brünger, A.T. and Karplus, M. (1985) *J. Mol. Biol.*, **186**, 435–455.
- Clore, G.M., Brünger, A.T., Karplus, M. and Gronenborn, A.M. (1986a) *J. Mol. Biol.*, **191**, 523–551.
- Clore, G.M., Nilges, M., Sukumaran, D.K., Brünger, A.T., Karplus, M. and Gronenborn, A.M. (1986b) *EMBO J.*, **5**, 2729–2735.

- Clore, G.M., Gronenborn, A.M., James, M.N.G., Kjaer, M., McPhalen, C.A. and Poulsen, F.M. (1987a) *Protein Engineering*, **1**, 313–318.
- Clore, G.M., Sukumaran, D.K., Nilges, M. and Gronenborn, A.M. (1987b) *Biochemistry*, **26**, 1732–1745.
- Clore, G.M., Sukumaran, D.K., Nilges, M., Zarbock, J. and Gronenborn, A.M. (1987c) *EMBO J.*, **6**, 529–537.
- Clore, G.M., Gronenborn, A.M., Nilges, M., Sukumaran, D.K. and Zarbock, J. (1987d) *EMBO J.*, **6**, 1833–1842.
- Clore, G.M., Gronenborn, A.M., Nilges, M. and Ryan, C.A. (1987e) *Biochemistry*, in press.
- Crippen, G.M. and Havel, T.F. (1975) *Acta Crystallogr.*, **A34**, 282–284.
- Feldman, R.J., Brooks, B.R. and Lee, B. (1986) *Tools for Each Age: Understanding Protein Architecture Through Simulated Unfolding*. Division of Computer Research and Technology, National Institutes of Health, Bethesda, MD.
- Havel, T.F. (1986) *DISGEO, Quantum Program Chemistry Exchange Program No. 507*. Indiana University, IN.
- Havel, T.F., and Wüthrich, K. (1984) *Bull. Math. Biol.*, **45**, 673–698.
- Havel, T.F. and Wüthrich, K. (1985) *J. Mol. Biol.*, **182**, 281–294.
- Havel, T.F., Kuntz, I.D. and Crippen, G.M. (1983) *Bull. Math. Biol.*, **45**, 665–720.
- Jonassen, I. (1980) *Carlsberg Res. Commun.*, **45**, 47–58.
- Jeener, J., Meier, B.H., Bachmann, P. and Ernst, R.R. (1979) *J. Chem. Phys.*, **71**, 4546–4553.
- Jones, T.A. (1978) *J. Appl. Crystallogr.*, **11**, 268–272.
- Kaptein, R., Zuiderweg, E.R.P., Scheek, R.M., Boelens, R. and van Gunsteren, W.F. (1985) *J. Mol. Biol.*, **182**, 179–182.
- Kjaer, M. and Poulsen, F.M. (1987) *Carlsberg Res. Commun.*, in press.
- Kjaer, M., Kindler, J., Denys, L.A., Ludvigsen, S.J. and Poulsen, F.M. (1987) *Carlsberg Res. Commun.*, in press.
- Laskowski, M., Jr, and Kato, I. (1980) *Annu. Rev. Biochem.*, **49**, 593–626.
- Levitt, M. (1983) *J. Mol. Biol.*, **170**, 723–764.
- Macura, C., Huang, Y., Suter, D. and Ernst, R.R. (1981) *J. Magn. Resonance*, **43**, 259–281.
- McPhalen, C.A. and James, M.N.G. (1987) *Biochemistry*, **226**, 261–269.
- McPhalen, C.A., Svendsen, I., Jonassen, I. and James, M.N.G. (1985) *Proc. Natl. Acad. Sci. USA*, **82**, 7242–7246.
- Pardi, A., Billeter, M. and Wüthrich, K. (1984) *J. Mol. Biol.*, **180**, 741–750.
- States, D.J., Haberkorn, R.A. and Ruben, D.J. (1982) *J. Magn. Resonance*, **48**, 286–292.
- Svendsen, I., Jonassen, I., Jejgaard, J. and Boisen, S. (1980) *Carlsberg Res. Commun.*, **45**, 389–395.
- Williamson, M.P., Havel, T.F. and Wüthrich, K. (1985) *J. Mol. Biol.*, **182**, 295–315.
- Wüthrich, K., Billeter, M. and Braun, W. (1983) *J. Mol. Biol.*, **169**, 949–961.

Received on June 24, 1987